Morphology Control of Carbon, Silica, and Carbon/Silica Nanocomposites: From 3D Ordered Macro-/Mesoporous Monoliths to Shaped Mesoporous Particles[†]

Zhiyong Wang and Andreas Stein*

Department of Chemistry, University of Minnesota, Minneapolis, Minnesota 55455

We demonstrate that confinement of a concentrated triconstituent precursor solution (a soluble phenol-formaldehyde prepolymer, tetraethylorthosilicate, and the nonionic triblock copolymer F127) in a poly(methyl methacrylate) (PMMA) colloidal crystal template permits control over the external morphology of mesostructured products. It is possible to produce either monoliths with hierarchical porosity (ordered macropores from PMMA spheres and large mesopores from F127) or cubic and spherical mesoporous nanoparticles. The specific morphology depends on the concentration of F127 and on the presence of 1,3,5-trimethyl benzene (TMB) as an additive. At lower F127 content and without TMB, macroporous monoliths of the carbon/silica composite are obtained, which can be converted to carbon monoliths with dual porosity after the extraction of silica with hydrofluoric acid or to silica monoliths after calcination in air. Large worm-like mesopores are present in macropore walls. An increase in the F127 concentration leads to disassembly of the macroporous skeleton during pyrolysis and produces a bimodal mixture of uniformly sized cubic nanoparticles (ca. 120 nm edge lengths) and smaller spherical nanoparticles (ca. 55 nm diameters) (MSP-1). These nanoparticles are derived from the octahedral and tetrahedral holes in the colloidal crystal template through the solid-state disassembly of the inorganic skeleton. The addition of TMB changes the mechanism of nanoparticle formation. In this case, solvent-induced phase separation between the polymer template and the inorganic precursors occurs below 100 °C, which results in spherical nanoparticles (MSP-2), whose product diameters depend more critically on sample composition. Both MSP-1 and MSP-2 nanoparticles are mesoporous, but their textural properties vary significantly with type and composition. The MSP-1 particles keep their cubic shapes even after being heated at 1000 °C in an inert atmosphere.

Introduction

Advances in both soft and hard templating techniques have enabled syntheses of porous solids whose pore sizes, size-distributions, and geometries can be relatively well controlled. The field of porous materials has been driven by a broad range of applications, many of which rely on the incorporation of specific guests into pores of different sizes and on the transport of such guests through the pores (e.g., catalysis, separations, sensing). Composition also plays an important role, influencing physical properties and chemical reactivities of the material, as well as interfacial interactions. To optimize all of these properties for specific applications, it is necessary to be able to select the external sizes, shapes, and overall morphologies of the porous materials. For example, if guest transport is critical, small particle sizes permit shorter diffusion paths.[1] Shaped particles may facilitate the assembly of pieces into larger structures.[2–5] Larger monolithic pieces can be advantageous if a porous material needs to be incorporated into a device, for instance, when it is employed as an electrode,[6,7] a catalytic microreactor,[8,9] or as a membrane for separation.[10] Hierarchical structures can fulfill several of these criteria by providing both mesoporous components with nanometer dimensions and, at the same time, maintaining overall macroscopic dimensions for easier handling and perhaps greater structural uniformity.

Here, we present a synthetic approach to produce nano-structured materials that are either monolithic, containing designed porosity on multiple length scales, or are formed as porous nanoparticles with controllable shapes and sizes. The synthesis combines recently developed triconstituent self-assembly[11,12] with colloidal crystal templating,[13] template-guided disassembly,[14,15] and phase separation processes.[16]

† Part of the "Templated Materials Special Issue".
* To whom correspondence should be addressed. E-mail: stein@chem.umn.edu..
(1) Han, Y.; Ying, J. Y. *Angew. Chem., Int. Ed.* **2005,** *44,* 288–292.
(2) Kalsin, A. M.; Fialkowski, M.; Paszewski, M.; Smoukov, S. K.; Bishop, K. J. M.; Grazybowski, B. A. *Science* **2006,** *312,* 420–424.
(3) Manoharan, V. N.; Elsesser, M. T.; Pine, D. J. *Science* **2003,** *301,* 483–487.
(4) Shevchenko, E. V.; Talapin, D. V.; Kotov, N. A.; Stephen, O. B.; Murray, C. B. *Nature* **2006,** *439,* 55–59.
(5) Velikov, K. P.; Christova, C. G.; Dullens, R. P. A.; van Blaaderen, A. *Science* **2002,** *296,* 106–109.
(6) Lee, K. T.; Lytle, J. C.; Ergang, N. S.; Oh, S. M.; Stein, A. *Adv. Funct. Mater.* **2005,** *15,* 547–556.
(7) Lai, C.-Z.; Fierke, M. A.; Stein, A.; Buhlmann, P. *Anal. Chem.* **2007,** *79,* 4621–4626.
(8) Kirschning, A.; Altwicker, C.; Drager, G.; Harders, J.; Hoffmann, N.; Hoffmann, U.; Schonfeld, H.; Solodenko, W.; Kunz, U. *Angew. Chem., Int. Ed.* **2001,** *40,* 3995–3998.
(9) Ganley, J. C.; Riechmann, K. L.; Seebauer, E. G.; Masel, R. I. *J. Catal.* **2004,** *227,* 26–32.
(10) Hosoya, K.; Ogata, T.; Watabe, Y.; Kubo, T.; Ikegami, T.; Tanaka, N.; Minakuchi, H.; Nakanishi, K. *J. Chromatogr.* **2005,** *1073,* 123–126.
(11) Liu, R.; Shi, Y.; Wan, Y.; Meng, Y.; Zhang, F.; Gu, D.; Chen, Z.; Tu, B.; Zhao, D. *J. Am. Chem. Soc.* **2006,** *128,* 11652–11662.

On the basis of the triconstituent self-assembly reaction, products composed of carbon, silica, or mixed carbon–silica nanostructures are obtained by this method and can, in principle, be converted to many other compositions through well-established nanocasting methods.[17–19]

Triconstituent self-assembly normally involves the combination of two polymerizable precursors (e.g., a soluble resol polymer and a silicon alkoxide) with a triblock copolymer as a template.[11] When used in very dilute form (e.g., in ethanol), the precursor solution self-assembles into mesostructures as the solvent evaporates (evaporation-induced self-assembly or EISA) and the precursors condense. When the resulting composite is pyrolyzed in an inert atmosphere, the triblock copolymer is removed and a mesoporous carbon/silica composite is formed. The silica component can be eliminated by etching to produce mesoporous carbon. Alternately, carbon is removable through calcination to yield mesoporous silica. The products are usually thin films or powdered particles.[11,20]

In this study, we demonstrate that a triconstituent precursor in a more concentrated form can be infiltrated into a colloidal crystal template and processed to achieve mesoporous products in multiple forms: extended millimeter-sized monoliths as well as discrete cubic or spherical particles with dimensions on the order of 50–150 nm. In addition to the mesopores resulting from the triblock copolymer template, the monoliths contain periodic arrays of uniform macropores with sizes dictated by the colloidal crystal template. In pure silica form, inverse-opal monoliths with this kind of hierarchical porosity have been prepared by a number of routes.[21–27] Such structures have also been translated into carbon monoliths with hierarchical porosity by nanocasting, a process in which mesopores are infiltrated with polymeric phases, which are carb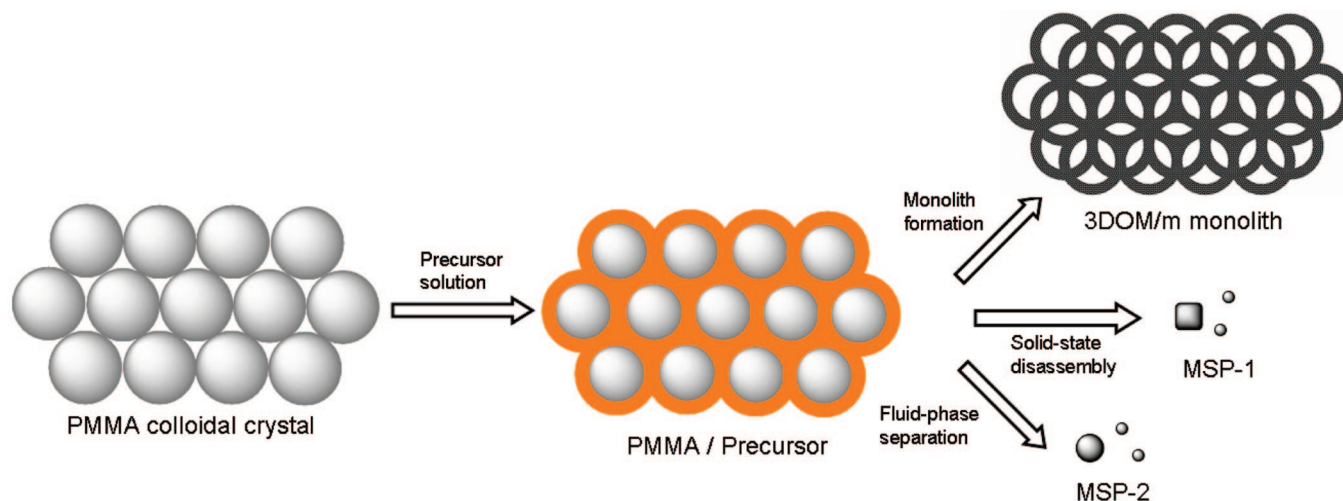onized before the silica mold is etched away.[19,28,29] However, the triconstituent precursor approach is more direct than nanocasting and decreases the synthesis time significantly.

The other morphologies achieved by the colloidal crystal templating process include small mesoporous cubes and spheres. Mesoporous particles have attracted much interest because of their potential applications in drug and gene delivery, enzyme immobilization, adsorption, and catalysis.[14,30–37] Conventionally, mesoporous silica spheres have been prepared by modified Stöber syntheses[1,38] and mesoporous carbon spheres by nanocasting methods that employ the silica spheres as a mold.[39] In the current work, the spherical particles are formed either by solvent-induced phase separation between the polymeric colloidal crystal template and the precursor mixture[40] or by disassembly and annealing of the templated inverse-opal structure.[14] Templated disassembly to produce mesoporous silica cubes from a biconstituent precursor has recently been communicated.[14] Bimodal sets of uniformly sized cubes and smaller tetrapods result from replicas of the octahedral and tetrahedral holes, respectively, in the face-centered cubic (fcc) colloidal crystal template. These shapes are kinetically stabilized and can convert to more spherical forms upon extended calcination. In the published synthesis, disassembly occurred only under specific conditions, which required a weak-acid catalyst for silica condensation. The mesoporous particles could be further used as nanocasting molds for carbon cubes and tetrapods. However, the triconstituent method illustrated here is a more direct route to carbon and carbon–silica composite phases and provides a greater yield of carbon products with less effort. Furthermore, it does not rely on a weak-acid catalyst that was necessary in the previous system.

The synthesis steps to obtain either monolithic products or mesostructured particles (MSP) are outlined in Scheme 1. Face-centered cubic colloidal crystals of monodisperse poly(methyl methacrylate) (PMMA) spheres are infiltrated with a clear precursor solution containing silica and carbon sources and a surfactant. After curing and carbonization, PMMA and the surfactant decompose and leave behind a porous carbon/silica nanocomposite monolith, that is, a three-dimensionally ordered

(12) Kang, Y.-S.; Lee, H. I.; Zhang, Y.; Han, Y. J.; Yie, J. E.; Stucky, G. D.; Kim, J. M. *Chem. Commun.* **2004**, 1524–1525.
(13) Holland, B. T.; Blanford, C. F.; Stein, A. *Science* **1998**, *281*, 538–540.
(14) Li, F.; Wang, Z.; Stein, A. *Angew. Chem., Int. Ed.* **2007**, *46*, 1885–1888.
(15) Warren, S. C.; DiSalvo, F. J.; Wiesner, U. *Nat. Mater.* **2007**, *6*, 156–161.
(16) Chen, Y.; Ford, W. T.; Materer, N. F.; Teeters, D. *J. Am. Chem. Soc.* **2000**, *122*, 10472–10473.
(17) Ryoo, R.; Joo, S. H.; Jun, S. *J. Phys. Chem. B* **1999**, *103*, 7743–7746.
(18) Yang, H.; Zhao, D. *J. Mater. Chem.* **2005**, *15*, 1217–1231.
(19) Wang, Z.; Li, F.; Ergang, N. S.; Stein, A. *Chem. Mater.* **2006**, *18*, 5543–5553.
(20) Zhang, F.; Meng, Y.; Gu, D.; Yan, Y.; Yu, C.; Tu, B.; Zhao, D. *J. Am. Chem. Soc.* **2005**, *127*, 13508–13509.
(21) Li, F.; Wang, Z.; Ergang, N. S.; Fyfe, C. A.; Stein, A. *Langmuir* **2007**, 3996–4004.
(22) Antonietti, M.; Berton, B.; Goeltner, C.; Hentze, H. P. *Adv. Mater.* **1998**, *10*, 154–159.
(23) Danumah, C.; Vaudreuil, S.; Bonneviot, L.; Bousmina, M.; Giasson, S.; Kaliaguine, S. *Microporous Mesoporous Mater.* **2001**, *44–45*, 241–247.
(24) Sel, O.; Kuang, D.; Thommes, M.; Smarsly, B. *Langmuir* **2006**, *22*, 2311–2322.
(25) Villaescusa, L. A.; Mihi, A.; Rodriguez, I.; Garcia-Bennett, A. E.; Miguez, H. *J. Phys. Chem. B* **2005**, *109*, 19643–19649.
(26) Kuang, D.; Brezensinski, T.; Smarsly, B. *J. Am. Chem. Soc.* **2004**, *126*, 10534–10535.
(27) Smarsly, B.; Polarz, S.; Antonietti, M. *J. Phys. Chem. B* **2001**, *105*, 10473–10483.
(28) Deng, Y.; Liu, C.; Yu, T.; Liu, F.; Zhang, F.; Wan, Y.; Zhang, L.; Wang, C.; Tu, B.; Webley, P. A.; Wang, H.; Zhao, D. *Chem. Mater.* **2007**, *19*, 3271–3277.
(29) Chai, G. S.; Shin, I. S.; Jong-Sung, Y. *Adv. Mater.* **2004**, *16*, 2057–2061.
(30) Djojoputro, H.; Zhou, X. F.; Qiao, S. Z.; Wang, L. Z.; Yu, C. Z.; Lu, G. Q. *J. Am. Chem. Soc.* **2006**, *128*, 6320–6321.
(31) Alonso, B.; Clinard, C.; Durand, D.; Veron, E.; Massiot, D. *Chem. Commun.* **2005**, 1746–1748.
(32) Lefevre, B.; Galarneau, A.; Jiapichella, J.; Petitto, C.; Di Renzo, F.; Fajula, F. *Chem. Mater.* **2005**, *17*, 601–607.
(33) Wang, Y.; Yu, A.; Caruso, F. *Angew. Chem., Int. Ed.* **2005**, *44*, 2888–2892.
(34) Wang, J.; Xia, Y.; Wang, W.; Mokaya, R.; Poliakoff, M. *Chem. Commun.* **2005**, 210–212.
(35) Wang, Y.; Caruso, F. *Chem. Mater.* **2005**, *17*, 953–961.
(36) Zhao, D.; Sun, J.; Li, Q.; Stucky, G. D. *Chem. Mater.* **2000**, *12*, 275–279.
(37) Zhu, Y.; Shi, J.; Shen, W.; Dong, X.; Feng, J.; Ruan, M.; Li, Y. *Angew. Chem., Int. Ed.* **2005**, *44*, 5083–5087.
(38) Suzuki, K.; Ikari, K.; Imai, H. *J. Am. Chem. Soc.* **2004**, *126*, 462–463.
(39) Xia, Y.; Yang, Z.; Mokaya, R. *J. Phys. Chem. B* **2004**, *108*, 19293–19298.
(40) Silveira, K. F.; Yoshida, I. V. P.; Nunes, S. P. *Polymer* **1995**, *36*, 1425–1434.

Scheme 1. Synthesis Steps for the 3D Ordered Macro-/Mesoporous (3DOM/m) Monoliths and for Mesostructured Particles (MSP)[a]

[a] Precursor solution is composed of hydrolyzed tetraethylorthosilicate (TEOS), phenol-formaldehyde prepolymer (PF), and surfactant, Pluronic F127. For the synthesis of MSP-2 particles, trimethylbenzene (TMB) is added to this precursor solution. PMMA colloidal crystal monoliths are infiltrated with this precursor solution, which is then thermally polymerized at 100 °C. After carbonization at 900 °C, carbon/silica nanocomposites 3DOM/m C-SiO₂, MSP-1-C-SiO₂, and MSP-2-C-SiO₂ are produced. 3DOM/m C monoliths, MSP-1-C, or MSP-2-C samples are obtained after the removal of silica by hydrofluoric acid. Silica counterparts are prepared by calcination in air at 550 °C. Refer to the text for experimental details.

macroporous product with mesoporous walls (3DOM/m monolith). The well interconnected macropores and mesopores are generated from the previously occupied positions of PMMA and surfactant, respectively. Upon increasing the surfactant concentration in the precursor solution, the second morphology, bimodally dispersed mesoporous particles (MSP-1) are obtained, which include larger nanocubes and smaller nanospheres. If instead an organic cosolvent is added, only nanospheres (MSP-2) are formed, with a bimodal size distribution. Silica can remain in these products as a structural support, or it can be removed by extraction with hydrofluoric acid, to produce self-standing porous carbon structures. Alternatively, purely siliceous products are created if the carbon component is eliminated by calcination.

Experimental Section

Chemicals. Chemicals used in this experiment were obtained from the following sources: 2,2′-azobis(2-methyl propionamidine) dihydrochloride (AMPD) initiator (97%), methyl methacrylate monomer (MMA) (99%), tetraethyl orthosilicate (TEOS, 98%), and 1,3,5-trimethylbenzene (TMB or mesitylene, 98%) were purchased from Aldrich. Phenol (ACS reagent) and formaldehyde (37% aqueous solution) were from Fisher Scientific. Hydrochloric acid (37%), hydrofluoric acid (48%), and sodium hydroxide were from Mallinckrodt Chemicals. Pluronic F127 (a difunctional nonionic ethylene oxide/propylene oxide block copolymer surfactant, $EO_{97}PO_{69}EO_{97}$, terminating in primary hydroxyl groups, average molecular weight 12600) was received as a gift from BASF. All of the chemicals were used without further purification.

Preparation of PMMA Monoliths. In this study, PMMA spheres were prepared by emulsifier-free emulsion polymerization of MMA at 70 °C with AMPD as an initiator, as described elsewhere.[41] The resulting PMMA sphere suspension was transferred to a glass crystallization dish and stored for several weeks

at room temperature without agitation. After the evaporation of water, PMMA spheres sedimented on the bottom of the container, forming opalescent colloidal crystal pieces.

Synthesis of 3DOM/m C-SiO₂ Monoliths. For the synthesis of 3DOM/m C-SiO₂ monoliths, a 50 wt% phenol–formaldehyde (PF) prepolymer solution in ethanol was first prepared as reported elsewhere.[11] For the precursor solution, 2.0 g TEOS was mixed with 1.0 g of 0.2 M HCl(aq) under vigorous stirring for 10–15 min at room temperature (RT) until a clear colorless solution was obtained. PF (2.0 g) prepolymer solution was then added, and the mixture was further stirred until it became homogeneous. A clear precursor solution formed after the addition of 2.5 g F127 and stirring overnight. Next, the precursor solution composed of silicate, PF prepolymer, and surfactant was added to a beaker containing the PMMA monoliths. Care was taken to keep the solution level below the top of the PMMA monoliths. The beaker was covered with Parafilm. Complete infiltration of the precursor solution into PMMA took about 24 h. After excess solution was wiped off the monoliths, these pieces were placed in a vacuum chamber for 2–3 h at RT to remove the solvent. The monoliths were then transferred to a plastic bottle and heated in an oven at 100 °C for 24 h to induce thermal polymerization (bottle capped). The composite monoliths were carbonized under flowing N₂ (1 L min⁻¹) at 400 °C for 3 h and then at 900 °C for another 2 h with a heating rate of 1 °C min⁻¹.
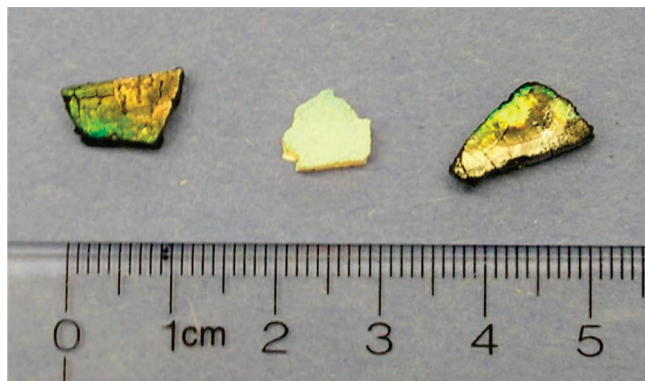
Synthesis of 3DOM/m C Monoliths. Silica was removed from the 3DOM/m C-SiO₂ monoliths by immersing them in 10 wt% hydrofluoric acid solution for 24 h, followed by extensive washing with DI water. (CAUTION!! HF solution is extremely dangerous and corrosive and must be handled according to MSDS procedures.) Finally, the monoliths were dried at 100 °C overnight.

Synthesis of 3DOM/m SiO₂ Monoliths. Carbon was removed from the 3DOM/m C-SiO₂ monoliths by calcination in flowing air (1 L min⁻¹) at 550 °C for 5 h. White monolithic products with opalescence were obtained.

Syntheses of MSP-1 and MSP-2 Particles. Typical syntheses of MSP-1 nanoparticles required small modifications of the recipe for 3DOM/m C-SiO₂. TEOS (2.0 g) was hydrolyzed in 1.0 g of

(41) Schroden, R. C.; Al-Daous, M.; Sokolov, S.; Melde, B. J.; Lytle, J. C.; Stein, A.; Carbajo, M. C.; Fernandez, J. T.; Rodriguez, E. E. *J. Mater. Chem.* **2002**, *12*, 3261–3327.

Figure 1. Photograph of 3DOM/m C-SiO$_2$ (left), 3DOM/m SiO$_2$ (center), and 3DOM/m C (right) monoliths.

0.2 M HCl(aq) under stirring at RT, followed by the addition of 2.0 g PF prepolymer solution (50 wt% solution in ethanol, as described above). A transparent solution was obtained after adding 4.0–4.5 g Pluronic F127 and stirring overnight. For the synthesis of MSP-2, 2.0 g F127 was used and 0.8 g TMB was added. The solution was further stirred overnight at RT. Next, PMMA monoliths were infiltrated with these precursor solutions by a method similar to that for the 3DOM/m materials. Excess solution was wiped off the monoliths before these were transferred to a plastic bottle and heated in an oven at 100 °C for 24 h (bottle capped). The composite monoliths were carbonized under N$_2$ flow (1 L min^{-1}) at 400 °C for 3 h and then at 900 °C for another 2 h with a heating rate of 1 °C min^{-1}. This carbonized sample. containing both carbon and silica, is denoted as MSP-x-C-SiO$_2$ (x = 1, 2). Silica samples MSP-x-SiO$_2$ were prepared by burning off carbon in the composite at 550 °C for 5 h in flowing air (1 L min^{-1}) with a heating rate of 1 °C min^{-1}. Carbon samples MSP-x-C were obtained by soaking the composite at RT in a 10 wt% hydrofluoric acid solution for 24 h inside a polypropylene bottle, followed by extensive washing with DI water to remove silica. Finally, samples were dried at 100 °C overnight.

Characterization. Scanning electron microscopy (SEM) images were obtained with a JEOL 6700 scanning electron microscope at an accelerating voltage of 5 kV. Samples were ground to a powder and then mounted on an aluminum stub with conductive carbon tape. For electrically nonconductive samples such as MSP-x-SiO$_2$, a 5 nm platinum coating was applied before SEM analysis. Transmission electron microscopy (TEM) was conducted on a JEOL model JEM-1210 electron microscope operated at 120 kV. All of the samples were crushed to a powder and sonicated in acetone for several hours before TEM analysis. They were drop-dried from acetone onto TEM grids. Nitrogen-sorption measurements were performed on a Micromeritics ASAP 2000 gas sorptometer. Samples were degassed at 0.003 mm Hg for at least 12 h at 200 °C. Specific surface areas were calculated by the Brunauer–Emmett–Teller (BET) method, and pore sizes and volumes were estimated from pore size distribution curves from the adsorption branches of the isotherms. Pore volumes were taken at the P/P$_0$ = 0.995 single point.

Results and Discussion

3DOM/m Monolith. As-synthesized 3DOM/m samples were monolithic with a typical thickness of ca. 3 mm and edge lengths from several millimeters to 1 centimeter on each side, as seen in Figure 1. As a result of their highly periodic macroporous structure, strong opalescence was observed in

daylight, superimposed on the natural black or white appearance of the carbonaceous and silica materials, respectively. The color of opalescence depended on the viewing angle. In this photograph (Figure 1), it is metallic green and yellow.

PMMA colloidal crystal monoliths with sphere diameters of 416 ± 11 nm were used as templates for the generation of both 3DOM/m monoliths and particles in the MSP-series (Figure S1 in the Supporting Information). After carbonization in nitrogen at 900 °C for 2 h, a three-dimensionally ordered macroporous (3DOM) network was observed by SEM in most regions of the 3DOM/m samples (part A of Figure 2). Macropore diameters and pore window sizes (openings between adjacent macropores) for 3DOM/m C-SiO$_2$ averaged 367 ± 4 and 126 ± 6 nm, respectively, as measured from the SEM image. The linear shrinkage was 12% from PMMA spheres to 3DOM/m C, which was similar to the shrinkage of typical 3DOM silica after calcination[42] but significantly lower than the value for 3DOM carbon we synthesized previously from precursors lacking the TEOS component.[6] 3DOM/m SiO$_2$ or 3DOM/m C monoliths were derived from the 3DOM/m C-SiO$_2$ composite by calcination in air at 550 °C for 5 h or by etching with hydrofluoric acid, respectively. Both the macropore sizes and window sizes decreased significantly from the 3DOM/m C-SiO$_2$ composite to 3DOM/m SiO$_2$, but the shrinkage for 3DOM/m C was comparatively small (parts B and C of Figure 2, Table 1). Further contraction of the silica network occurred during the oxidation process at 550 °C.
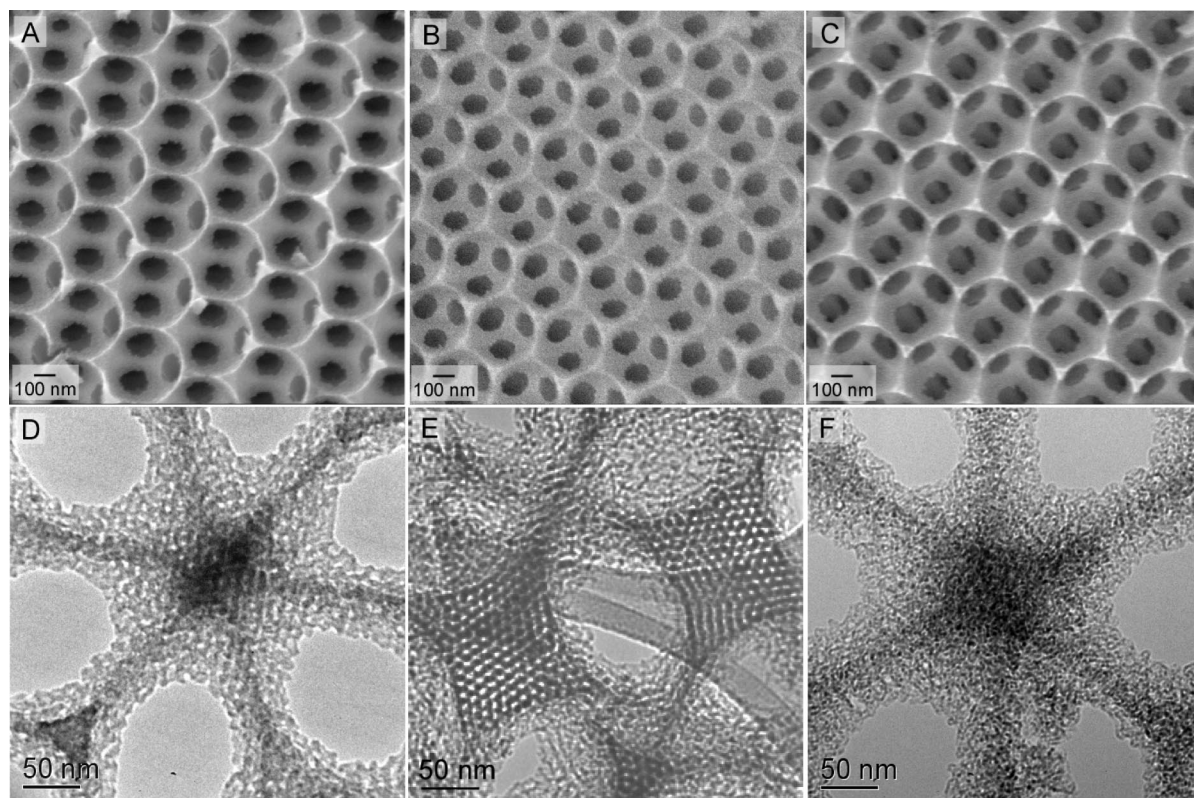
The internal wall structure of 3DOM/m monoliths was analyzed by transmission electron microscopy (parts D, E, and F of Figure 2). Images acquired at high magnification revealed worm-like mesoporous channels inside the 3DOM skeletons. For the 3DOM/m SiO$_2$ sample, some domains of ordered mesopore patterns were observed (part E of Figure 2). Mesopores were distributed evenly over the whole samples.

Nitrogen-sorption experiments were performed to further examine the porosity (Figure 3). The 3DOM/m monoliths exhibit reversible type-IV curves typical for mesoporous materials, albeit with relatively shallow slopes in both the adsorption and desorption branches.[43] Two hysteresis loops appear in the relative pressure ranges from 0.4–0.8 and 0.8–1.0 (P/P$_0$), which are related to the filling and emptying of mesopores by capillary condensation.[44] The first loop at 0.4–0.8 is due to capillary condensation within mesopores generated by the surfactant F127. The second loop may arise from the rough texture on the macropore wall surface, as evident in the TEM images (parts D, E, and F of Figure 2). 3DOM/m C possesses a specific BET surface area of 1900 m^2 g^{-1} and a pore volume of 1.25 cm^3 g^{-1}, values much higher than for our previously synthesized 3DOM/m C

(42) Schroden, R. C.; Al-Daous, M.; Blanford, C. F.; Stein, A. *Chem. Mater.* **2002**, *14*, 3305–3315.

(43) Brunauer, S.; Deming, L. S.; Deming, W. S.; Teller, E. *J. Am. Chem. Soc.* **1940**, *62*, 1723–1732.

(44) Rouquerol, F.; Rouquerol, J.; Sing, K. *Adsorption by Powders and Porous Solids: Priciples, Methodology, Applications*; Academic Press: New York, 1999; p 20.

Figure 2. SEM images (A, B, and C) and TEM images (D, E, and F) of 3DOM/m C-SiO$_2$ (A and D), 3DOM/m SiO$_2$ (B and E), and 3DOM/m C (C and F) monoliths.

Table 1. Dimensional and Porosity Data for 3DOM/m Monoliths and MSP Particles

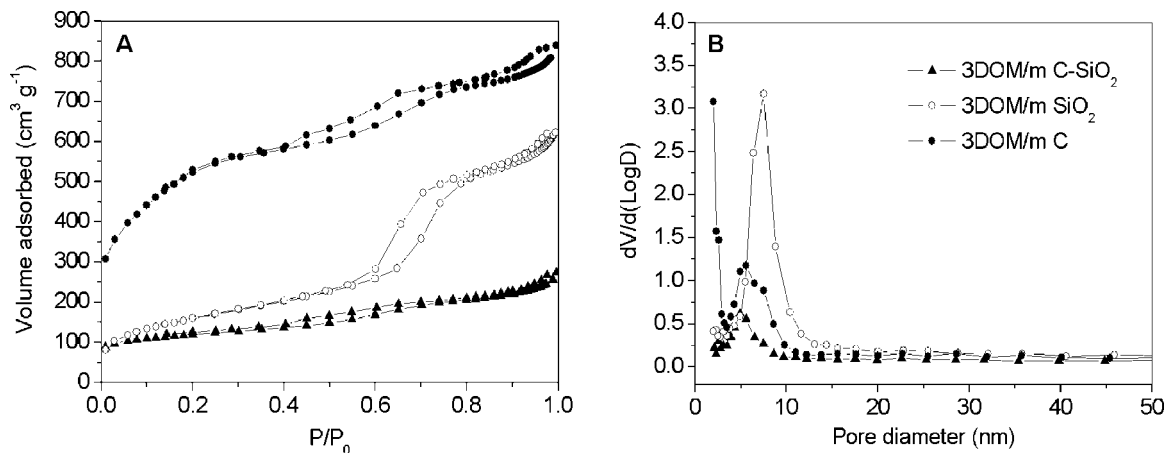| sample name	macropore/particle size (nm)^a	mesopore size (nm)^b	S_{BET} (m^2 g^{-1})	V_{pore} (cm^3 g^{-1})^c	$V_{mesopore}$ (%)^d	$V_{micropore}$ (%)^e
3DOM/m C-SiO$_2$	367 ± 4 126 ± 6	5.2	416	0.39	73	18
3DOM/m SiO$_2$	319 ± 7 119 ± 4	6.4, 7.5	584	0.93	98	N.A.^{h}
3DOM/m C (direct synthesis)^f	359 ± 4 127 ± 5	5.4, 7.3	1900	1.25	68	28
3DOM/m C (nanocast)^g	286 ± 2 100 ± 5	2.9	1261	0.93	81	17
MSP-1-C-SiO$_2$	120 ± 7 56 ± 7	~5	102	0.09	63	22
MSP-1-SiO$_2$	119 ± 6 56 ± 5	5.4	562	0.86	95	N.A.^{h}
MSP-1-C	120 ± 9 54 ± 7	~5	1180	0.66	64	31
MSP-2-C-SiO$_2$	152 ± 4 56 ± 3	5.6	298	0.25	68	26
MSP-2-SiO$_2$	119 ± 8 50 ± 3	6.5, 8.6	546	0.96	96	N.A.^{h}
MSP-2-C	140 ± 7 54 ± 3	5.9	1283	0.84	77	21

^{a} For 3DOM/m samples, the top and the bottom lines refer to the macropore and window sizes, respectively, averaged over 10–20 pores for each sample. For MSP samples, the top and the bottom lines refer to the sizes of the bimodal particles (diameters for spheres, edge lengths for cubes) averaged over several hundred particles for each sample. ^{b} Positions of peak maxima in the BJH pore size distribution curves calculated from adsorption isotherms. ^{c} Single-point total-pore volume at $P/P_0 = 0.995$. ^{d} Mesopore volumes used here are BJH cumulative adsorption pore volumes of pores between 2 and 50 nm. ^{e} This is calculated from the equation:$V_{micropore}(\%) = 100 \times (V_{pore} - V_{mesopore} - V_{macropore})/V_{pore}$. ^{f} 3DOM/m C monolith prepared by direct synthesis as described in this paper. ^{g} 3DOM/m C monolith prepared by nanocasting (ref 19 for details). ^{h} N.A. indicates that the micropore volume could not be calculated because the estimated $V_{mesopore}$ was larger than the estimated total-pore volume.

monolith (1261 m^2 g^{-1} and 0.93 cm^3 g^{-1}) that was prepared by a nanocasting route.[19] A significant fraction of the pore volume (28%) can be attributed to micropores (Table 1).
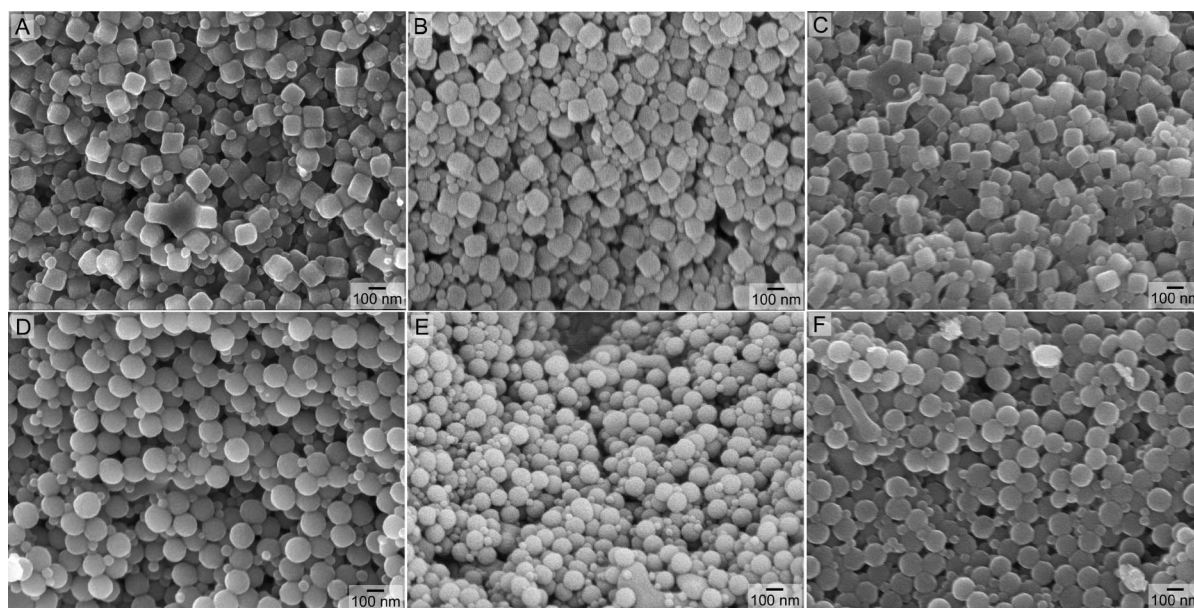
MSP-x Particles. Mesostructured particles were synthesized using a procedure similar to that for the 3DOM/m monoliths, except that the F127 concentration in the precursor solution was increased (for MSP-1) or TMB was added (for

MSP-2 with a slightly decreased F127 concentration). After carbonization, bimodally dispersed particles MSP-1-C-SiO$_2$ were observed by SEM (part A of Figure 4). Larger particles exhibited cubic shapes (120 ± 7 nm, edge length), whereas smaller ones (56 ± 7 nm, diameter) were more spherical. The formation of these particles is based on a similar disassembly mechanism proposed by us recently.[14] Connec-

Figure 3. Nitrogen-sorption isotherms (A) and pore-size distribution curves (B) calculated from adsorption branches by the BJH method for 3DOM/m monoliths. Triangles, open circles, and solid circles correspond to data traces for 3DOM/m C-SiO$_2$, 3DOM/m SiO$_2$, and 3DOM/m C, respectively.

Figure 4. SEM images of MSP-1-C-SiO$_2$ (A), MSP-1-SiO$_2$ (B), MSP-1-C (C), and MSP-2-C-SiO$_2$ (D), MSP-2-SiO$_2$ (E), and MSP-2-C (F).

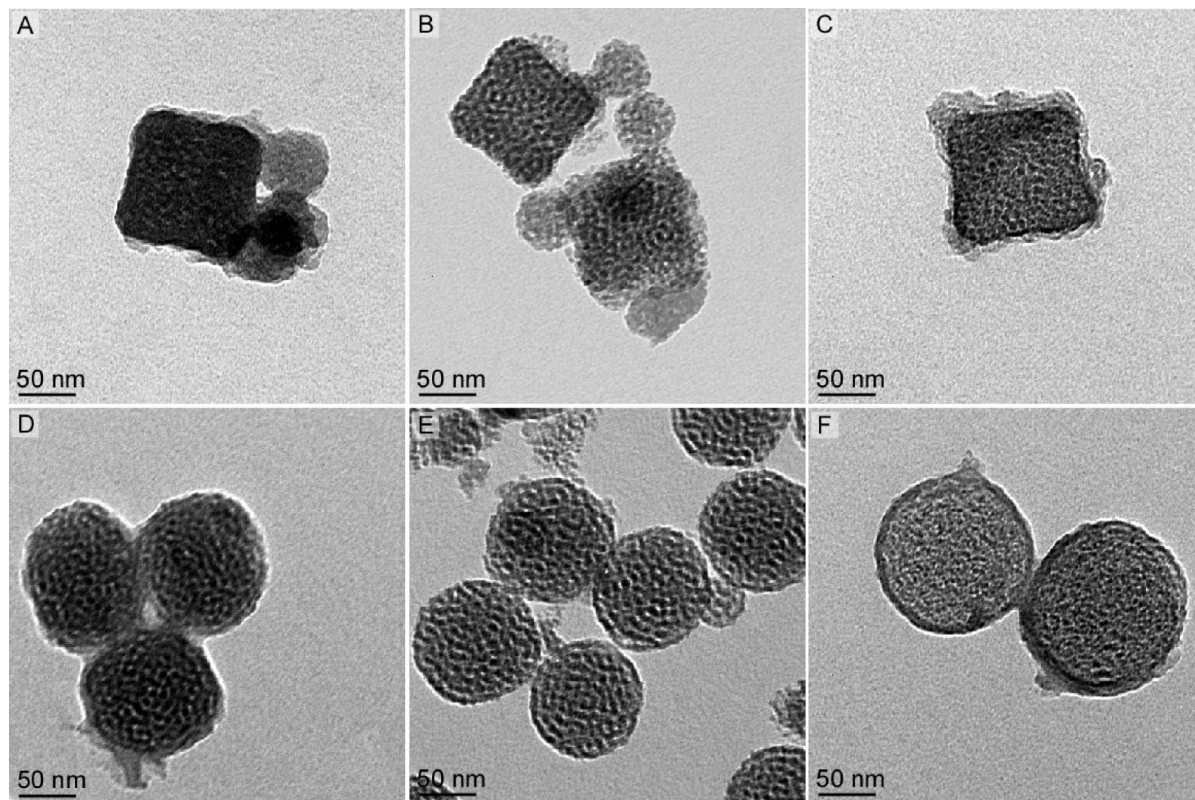tions between octahedral (O_h) and tetrahedral (T_d) centers, which are building units of the 3DOM structure, shrink during heating treatment and eventually disconnect, thereby generating the uniform bimodally distributed particles. After the removal of carbon or silica, the dimensions of the product particles did not change significantly (parts B and C of Figure 4, Table 1). Among 1150 particles counted from three SEM images of MSP-1-C-SiO$_2$, 401 particles were large and 749 were small. Within the error of the sampling technique, this ratio is close to the theoretical value of 1:2 for the ratio of the number of O_h centers to T_d centers. At lower F127 concentrations, 3DOM/m monoliths were formed and did not disassemble into individual nanoparticles.

For the synthesis of MSP-2 particles, a lower concentration of F-127 was used and 1,3,5-trimethylbenzene (TMB) was added to the precursor mixture. TMB is conventionally used as an auxiliary organic agent to swell surfactant micelles and produce mesoporous materials with larger pores.[45,46] During our study, we found that TMB in the original precursor solution was capable of inducing morphology changes in the products. With the assistance of TMB, uniform bimodally

dispersed spheres with sizes of 152 ± 4/56 ± 3, 119 ± 8/50 ± 3, and 140 ± 7/54 ± 3 nm could be observed for MSP-2-C-SiO$_2$, MSP-2-SiO$_2$ and MSP-2-C, respectively (parts D, E, and F of Figure 4), even at a low surfactant concentration compared to the MSP-1 system (mass of F127 from 2.0–4.5 g). The 1228 particles that were counted for the MSP-2-C-SiO$_2$ sample from three SEM images included 417 large spheres and 811 small spheres. This ratio is again close to the theoretical value of 1:2 for octahedral/tetrahedral holes.[14] Besides these spheres, a small number of rod-like particles were also seen in the carbon sample (part F of Figure 4). Some rods were even observed at an early stage of thermal treatment (100 °C). They probably originate from defects in the original colloidal crystal template.

(45) Beck, J. S.; Vartuli, J. C.; Roth, W. J.; Leonowicz, M. E.; Kresge, C. T.; Schmitt, K. D.; Chu, C. T.-W.; Olson, D. H.; Sheppard, E. W.; McCullen, S. B.; Higgins, J. B.; Schlenker, J. L. *J. Am. Chem. Soc.* **1992**, *114*, 10834–10843.
(46) Zhao, D.; Huo, Q.; Feng, J.; Chmelka, B. F.; Stucky, G. D. *J. Am. Chem. Soc.* **1998**, *120*, 6024–6036.
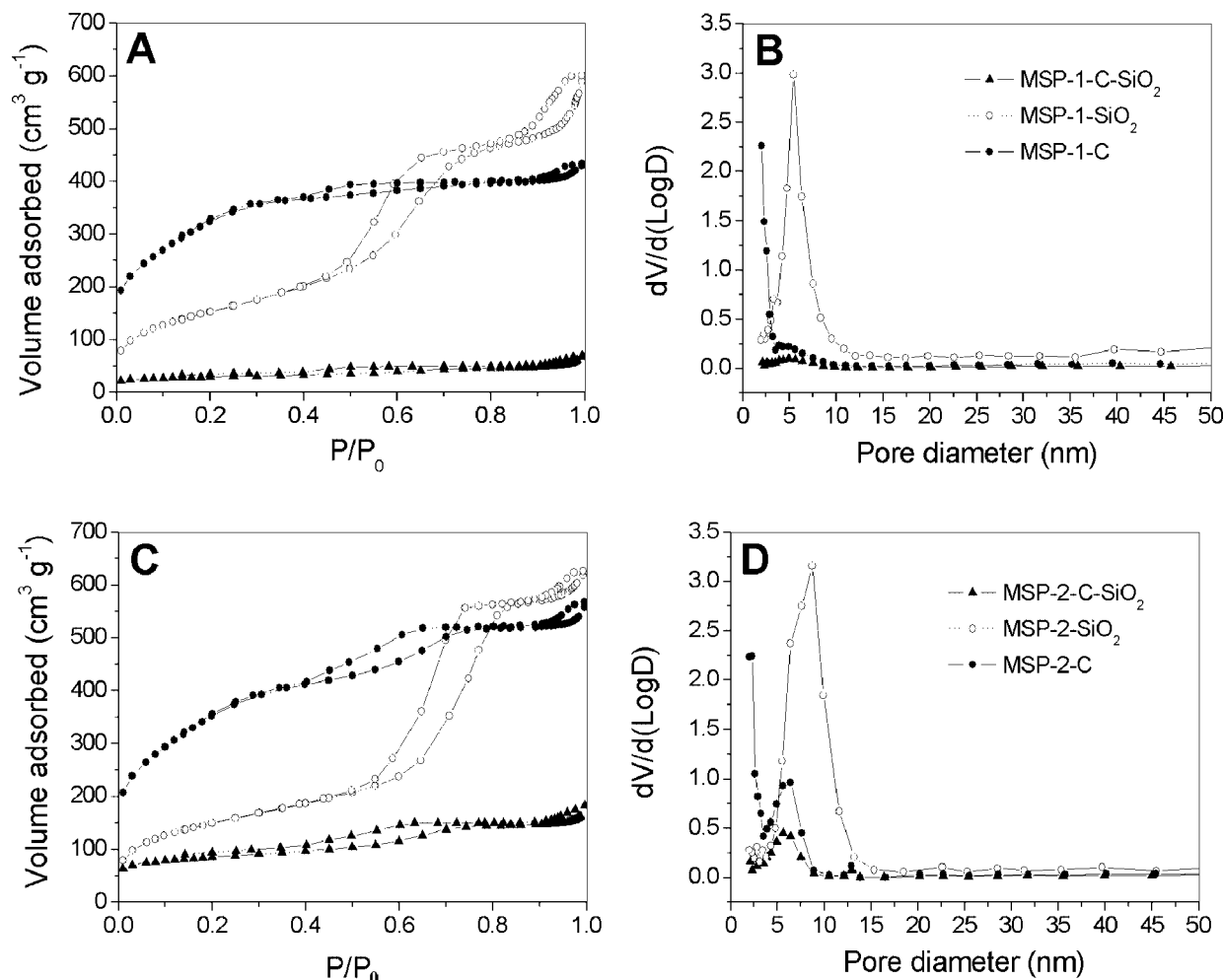
Figure 5. TEM images of MSP-1-C-SiO$_2$ (A), MSP-1-SiO$_2$ (B), MSP-1-C (C) and MSP-2-C-SiO$_2$ (D), MSP-2-SiO$_2$ (E), and MSP-2-C (F).

TEM images provide further details about the structure of these particles. The larger particles in MSP-1-C-SiO$_2$ have a cubic appearance, and many are surrounded by a thin irregular surface coating that may have resulted from partial precursor penetration into the surface of PMMA spheres (part A of Figure 5). This roughened surface character is typical for MSP-*x* particles. After calcination at 550 °C in air, the cubic and spherical shapes were maintained in the final silica particles. Mesopores could be more clearly observed in both the cubes and the smaller spheres because of contrast enhancement after carbon removal (part B of Figure 5). When HF etching was applied instead of calcination, mesoporous carbon products were generated with the same shapes (part C of Figure 5). Particle agglomeration was less pronounced for MSP-1-SiO$_2$ than MSP-1-C-SiO$_2$ and MSP-1-C. Similar to MSP-1, MSP-2 particles also showed mesostructures under TEM, and a wispy surface layer was observed on MSP-2-C-SiO$_2$ composite spheres (part D of Figure 5). After carbon was burned off, MSP-2-SiO$_2$ spheres were obtained whose mesopores could be distinctly observed in the TEM image (part E of Figure 5). When HF etching was employed on MSP-2-C-SiO$_2$ to remove silica, the resulting carbon spheres were also mesoporous (part F of Figure 5 and Table 1), but in the TEM image, a darker, presumably denser surface layer was detected. This carbon-rich phase may have resulted from incomplete carbon removal from the PMMA-rich phase, as this sample had only been heated in an inert atmosphere.[47] A similar, though less-pronounced layer could also be observed for MSP-1-C (part C of Figure 5).

(47) Yan, H.; Blanford, C. F.; Stein, A.; Smyrl, W. H. *Chem. Commun.* **2000**, 1477–1478.

Data describing the pore texture of the mesostructured particles on the basis of nitrogen-sorption experiments are listed in Table 1. As is characteristic for mesoporous materials, all of the MSP samples displayed isotherms resembling type-IV adsorption (parts A and C of Figure 6). Similar to the 3DOM/m monoliths, two distinct hysteresis loops were observed for all of the MSP samples. Besides surface roughness, interparticle porosity could have contributed to the occurrence of the second loops in MSP samples.[1] Interestingly, a bimodal mesopore distribution existed in MSP-2-SiO$_2$ particles, with a peak at 8.6 and a shoulder at ca. 6.5 nm (part D of Figure 6). The secondary porous structure probably resulted from pores introduced by the removal of the carbon component. The as-synthesized MSP-*x*-C-SiO$_2$ composites had much lower BET surface areas and pore volumes than their progenies, MSP-*x*-SiO$_2$ and MSP-*x*-C (Table 1), but internal mesopores derived from the surfactant template still contributed significantly to the surface areas of the composites, as nonporous particles of these dimensions would have estimated specific surfaces areas of only ca. 31–32 m^2 g^{-1}. Mesoporous carbon particles MSP-*x*-C exhibited lower total-pore volumes than MSP-*x*-SiO$_2$ particles, despite their higher BET surface areas over silica counterparts. The higher BET surface areas resulted from the decrease of mesopore sizes and the existence of a significant fraction of micropores. Micropores were also relatively abundant in the C/SiO$_2$ composites, but no micropores were detected in the pure silica samples (Table 1). MSP-2 particles that were synthesized using TMB as a swelling agent consistently exhibited larger mesopore sizes and volumes than the MSP-1 particle prepared without TMB.

Figure 6. Nitrogen-sorption isotherms (A, C) and pore-size distribution curves (B, D) calculated from adsorption branches by the BJH method for MSP-1 (A, B) and MSP-2 (C, D). Triangles, hollow circles, and solid circles correspond to data for carbon/silica composite samples (MSP-1-C-SiO₂ and MSP-2-C-SiO₂), silica particles (MSP-1-SiO₂ and MSP-2-SiO₂), and carbon particles (MSP-1-C and MSP-2-C), respectively.

Formation of the Macro-/Mesostructure in 3DOM/m Monoliths. Direct syntheses of mesoporous carbon thin films typically rely on an evaporation-induced self-assembly (EISA) process, and the mesostructure depends strongly on factors such as film thickness, substrate, relative humidity, and evaporation rates.[48–51] The beginning steps in the 3DOM/m monolith synthesis are similar to those in thin film preparations in terms of precursor solutions (e.g., a clear, homogeneous alcoholic solution). However, later stages involve different types of interplay among the system components and thus involve a significantly different mechanism of mesostructure formation. When the EISA process is applied to thin films, evaporation occurs in a relatively short time; thus self-assembly of surfactant micelles together with precursors is highly favored. In contrast, evaporation is much less efficient in monolithic systems such as precursor-infiltrated PMMA colloidal crystal pieces, which have very long diffusion-path lengths. Consequently, to attain ordered mesostructures, longer evaporation or auxiliary techniques such as evacuation are necessary to remove short-chain alcoholic solvents (e.g., methanol or ethanol), which are believed to destroy the liquid crystalline phase.[52] Under reduced pressure, 3DOM/m silica monoliths with ordered mesopores were successfully synthesized by our group.[21] It is worth noting that in the current study of 3DOM/m monoliths, an ordered mesostructure was not observed as a prevailing morphology, although a variety of evaporation methods were attempted. One explanation could be that the spatial constraint imposed by the PMMA colloidal crystal hindered the alignment of F127 micelles to liquid crystalline domains during ethanol removal, because the void dimensions within the colloidal crystal were only 1 order of magnitude larger than the diameters of these micelles. Unlike the previous silica monolith syntheses, which employed small surfactants Brij56 and P123 (MW ∼680 and ∼5,800, respectively), preparation of the 3DOM/m C/SiO₂ composite monolith used F127 as a surfactant, which had a much higher molecular weight (MW ∼12600) and thus larger micelle sizes. As a result, confinement effects predominated in the

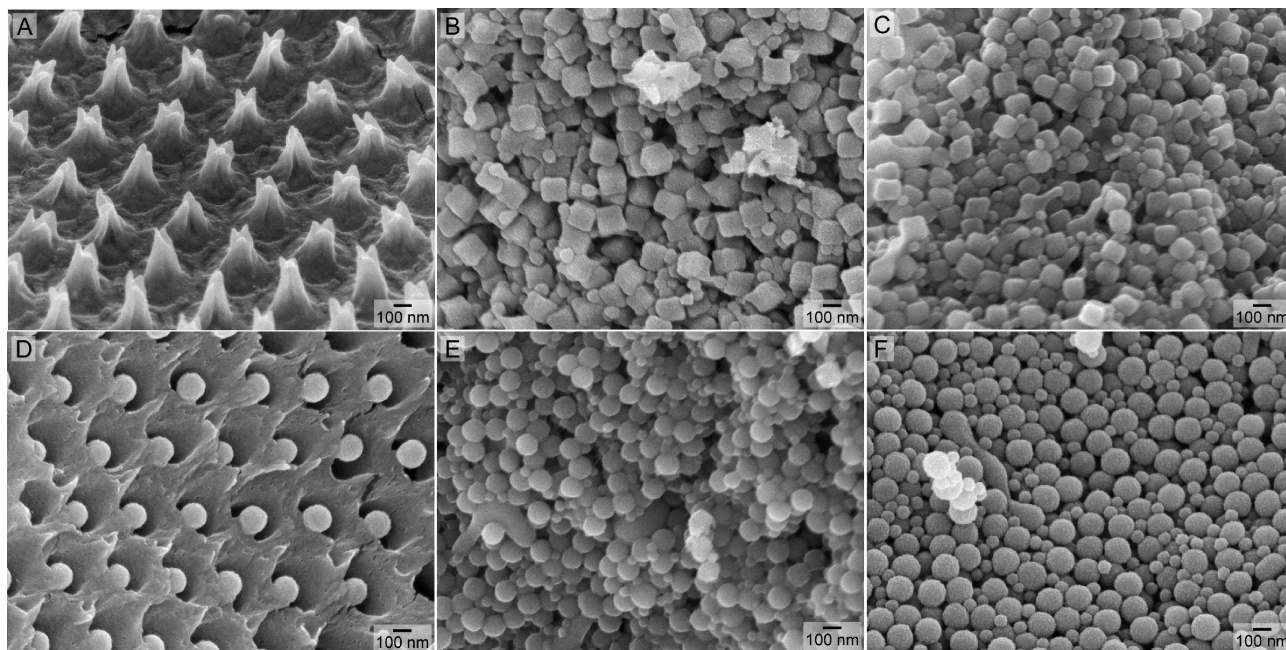(48) Tanaka, S.; Nishiyama, N.; Egashira, Y.; Ueyama, K. *Chem. Commun.* **2005**, 2125–2127.

(49) Meng, Y.; Gu, D.; Zhang, F.; Shi, Y.; Yang, H.; Li, Z.; Yu, C.; Tu, B.; Zhao, D. *Angew. Chem., Int. Ed.* **2005**, *44*, 2–8.

(50) Grosso, D.; Cagnol, F.; Soler-Illia, G. J. D. A. A.; Crepaldi, E. L.; Amenitsch, H.; Brunet-Bruneau, A.; Bourgeois, A.; Sanchez, C. *Adv. Funct. Mater.* **2004**, *14*, 309–322.

(51) Liang, C.; Dai, S. *J. Am. Chem. Soc.* **2006**, *128*, 5316–5317.

(52) Attard, G. S.; Glyde, J. C.; Goltner, C. G. *Nature* **1995**, *378*, 366–368.

Figure 7. SEM images of samples at various reaction stages. MSP-1: after 100 °C thermal curing for 24 h (A), after heat treatment at 400 °C for 3 h under N_2 flow (B), and after final carbonization at 900 °C for 2 h under N_2 flow (C). (D), (E), and (F) show the corresponding stages for MSP-2 for which TMB was used as an additive.

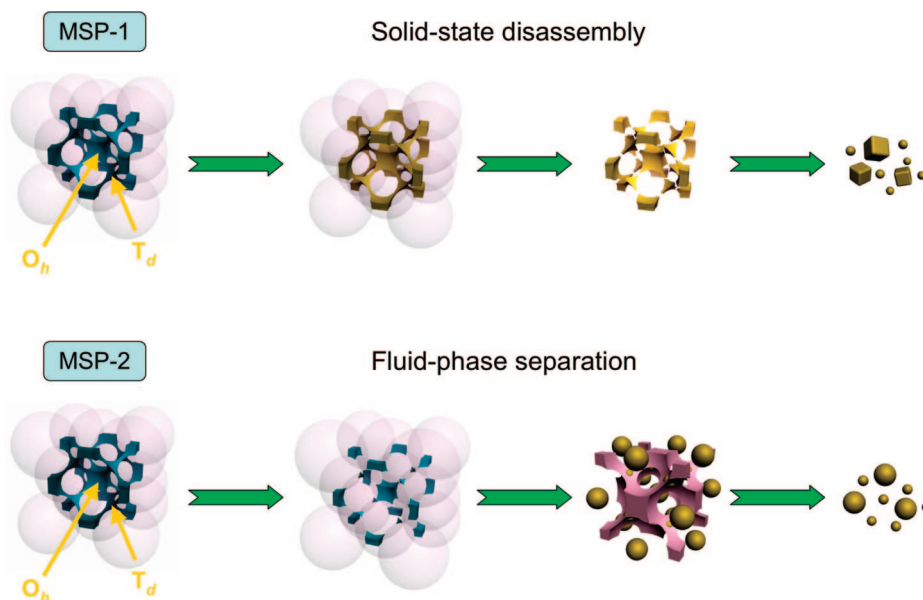arrangement of F127 micelles, and only disordered, worm-like mesostructures were obtained.

Formation Mechanisms for Mesoporous Particles. In a simpler system involving only a biconstituent precursor (TEOS and Brij 56), disassembly of a 3DOM structure into regular nanoparticles required the use of oxalic acid as a catalyst for hydrolysis and condensation of the siloxane.[14] Disassembly did not proceed with strong acids like HCl or HNO_3; instead, an interconnected inverse-opal structure was maintained. In contrast, we discovered in this study that disassembly occurred in the PF prepolymer/silicate/F127 triconstituent system without any additives or the use of oxalic acid. Simply elevating the surfactant (F127) concentration in the precursor solution yielded uniform nanocubes and smaller nanospheres in the final carbonized product. More interestingly, the addition of TMB into the precursor solution led to bimodally dispersed nanospheres with mesopores. Therefore, it is worth exploring the particle formation mechanism further to understand the morphology transformation process.

Three major stages during the synthesis may result in structural changes: (1) thermal curing at 100 °C for 24 h, (2) heat treatment at 400 °C for 3 h in N_2, and (3) carbonization at 900 °C for 2 h in N_2. SEM was used to follow the reaction progress. For the MSP-1 series (high surfactant concentration), after thermal curing at 100 °C (i.e., close to the glass transition temperature (T_g) of PMMA, 100–110 °C),[53] PMMA still maintained fcc packing. The lighter-colored, sea-anemone-shaped structures protruding from the spheres correspond to the original connections between adjacent spheres that were torn apart when the sample was cross-sectioned for SEM analysis (part A of
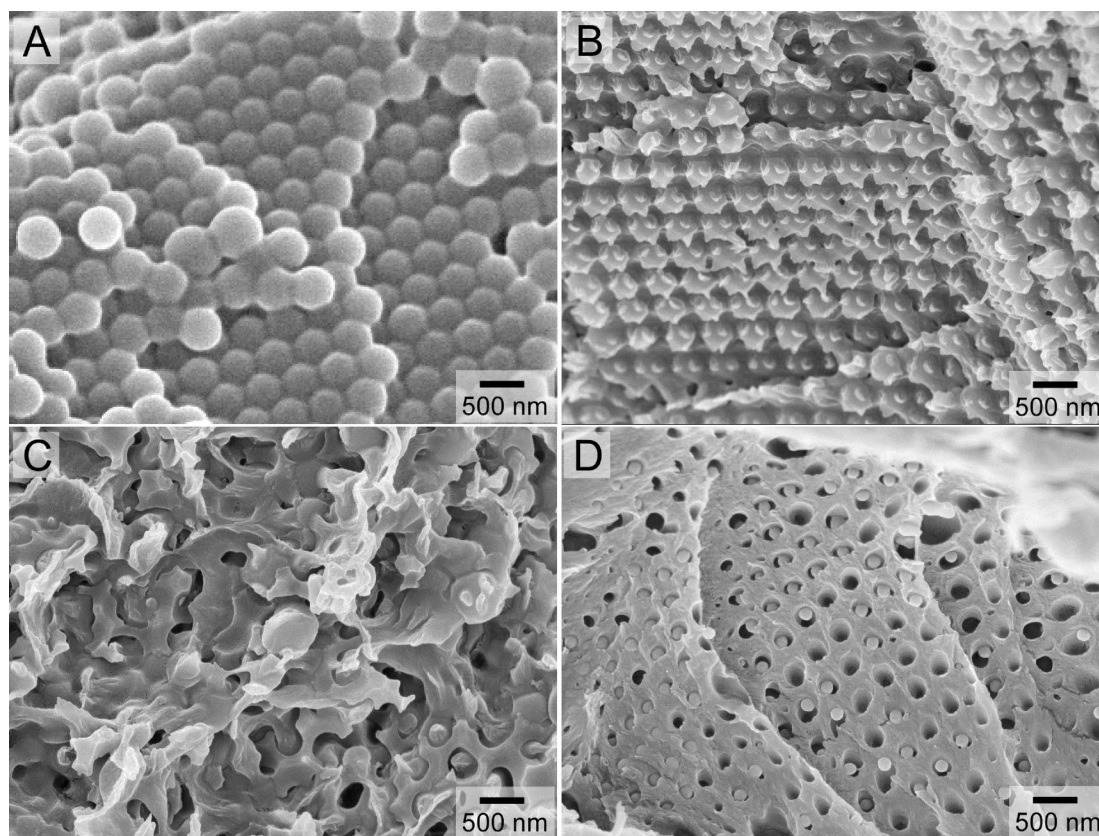
Figure 7). Interstitial voids within the colloidal crystal were completely filled with precursor species (PF prepolymer and silicates) and appeared to be continuous at this stage. After heat treatment at 400 °C in N_2, the 3DOM skeleton had disassembled to uniform bimodally dispersed particles: nanocubes from O_h centers and spheroids from T_d centers (part B of Figure 7), following a similar pathway as we proposed previously (Scheme 2).[14] However, particles were generated in a system using HCl instead of oxalic acid in the previous silica/Brij 56 system. Therefore, the formation of MSP-1 particles could be attributed to the high concentration of the surfactant. F127 has a low vapor pressure at 100 °C but decomposes almost completely after thermal treatment at 400 °C, leaving behind a more porous and weaker skeleton, which facilitates the cleavage of connecting parts between O_h and T_d centers. No significant morphology change was observed after carbonization at 900–1000 °C under N_2 (part C of Figure 7, Figure S2 in the Supporting Information).

The formation of MSP-2 appeared to follow a different pathway. Monodisperse spheres with diameters of 162 ± 4 nm were observed after the first thermal curing step at 100 °C (part D of Figure 7). More surprisingly, these spheres were confined inside an ordered macroporous matrix rather than an array of close-packed spheres. As discussed below, we believe that this is a structurally transformed PMMA matrix. The center-to-center distance of the adjacent macropores was 428 ± 12 nm, close to the sphere diameter in the original PMMA colloidal crystal (416 ± 11 nm). Smaller spheres with diameters of 63 ± 4 nm were also seen throughout the sample (Figure S3 in the Supporting Information). Because the TMB additive in the MSP-2 synthesis clearly altered the polymeric template below 100 °C, the morphology transition process was monitored in detail by

(53) Thompson, E. V. *J. Polym. Sci., Part A: Polym. Chem.* **1966**, *4*, 199–208.

Scheme 2. Proposed Mechanism for the Formation of MSP-1 and MSP-2 Nanoparticles[a]

[a] MSP-1: A PMMA colloidal crystal (pale-violet spheres) was first infiltrated with a precursor solution (blue) containing the PF prepolymer, F127, and silicates hydrolyzed from TEOS. The precursor occupied a continuous phase resembling a 3DOM structure that contains both O_h and T_d centers. This inorganic-rich phase remained continuous and condensed into a solid network (yellow) during heating. At a temperature between 100 and 400 °C, the network experienced sufficient stress due to shrinkage, to disassemble at the thinnest interconnecting points. Some rounding of the fragment edges and corners produced the cubes (from O_h centers) and the smaller spheres (originating from T_d centers). MSP-2: As above, a PMMA colloidal crystal (pale-violet spheres) was first infiltrated with a precursor solution (blue) that also contained TMB. When this composite was thermally cured at 100 °C for 24 h, TMB was released from F127 micelles and plasticized the PMMA spheres, which merged into each other to form a continuous inverse-opal-like phase. This process disconnected the precursor-rich phase at the O_h and T_d centers. At temperatures around 100 °C and/or after prolonged heating, further deformation of the PMMA-rich phase to a continuous macroporous network occurred, accompanied by shrinkage of the precursor phase to spheres. After heat treatment at 400 °C for 3 h in N_2, PMMA, TMB, and F127 were removed and PF/silica spheres were fully generated.

Figure 8. SEM micrographs of MSP-2 samples after thermal treatment at (A) 50 °C, (B) 60 °C, (C) 70 °C, and (D) 85 °C for 24 h each.

SEM (Figure 8). After a thermal treatment at 50 °C for 24 h, PMMA spheres remained mostly fcc packed (part A of

Figure 8). At 60 °C, spheres had begun to merge into a continuous phase, and small particles were observed on

PMMA spheres at the sites of the tetrahedral holes, suggesting that segregation of a precursor-rich phase was initiated (part B of Figure 8). Upon heating to 70 °C, the colloidal crystal completely lost its ordered structure to form a continuous skeleton, and particles of two sizes were now visible (part C of Figure 8). After heating at 85 °C, an ordered macroporous structure that encapsulated larger and smaller spheres was observed on ca. 30–40% of the cross section area (part D of Figure 8). This was similar to the structure in part D of Figure 7 obtained after heating to 100 °C. We were not able to analyze compositions at the resolution of individual spheres. However, considering volume fractions and sizes, it is plausible that the sphere phase contains mainly PF prepolymer and silicates, whereas the macroporous skeleton is a PMMA and TMB-rich phase. The surfactant, F127, may be distributed in both phases and also at the interface. Similar to MSP-1, bimodal distributions of nanospheres were fully generated after PMMA removal at 400 °C under N_2 (part E of Figure 7). The diameters of the large spheres changed from 162 ± 4 (after 100 °C treatment) to 158 ± 6 (after 400 °C treatment) and finally 143 ± 3 nm (after 900 °C carbonization), indicating volume shrinkage during each of these stages. Small spheres also shrunk from 63 ± 4 (100 °C) to 62 ± 8 (400 °C) to 52 ± 4 nm (900 °C).

On the basis of the above observations, a tentative mechanism for the formation of MSP-2 nanospheres is proposed (Scheme 2). Initially, PMMA monoliths are infiltrated with a precursor solution that occupies the voids and forms a 3D interconnected structure resembling a 3DOM (or inverse-opal) structure. TMB associates with the hydrophobic poly(propylene oxide) (PPO) segments of the surfactant (F127) micelles. During the early stages of thermal curing (room temperature to 85 °C), TMB is released from the PPO domains and then interacts with PMMA. A differential scanning calorimetry (DSC) measurement showed that the T_g of PMMA decreased to 74 °C after PMMA was soaked in TMB at 100 °C for 24 h inside a closed container. Because PMMA is plasticized by TMB at elevated temperature (part B of Figure S4 in the Supporting Information), adjacent spheres merge into a continuous polymer-rich phase, inducing neck growth between neighboring PMMA spheres. When the neck areas are sufficiently large, precursor sites in the O_h and T_d centers of the colloidal crystal voids are pinched off and become segregated from each other. Later, at higher temperatures and/or with prolonged heating, the precursor components contract to a spherical shape to minimize interfacial energies. At the same time, repulsions between the PMMA-rich phase and the precursor-rich spheres further deform the PMMA matrix to produce the observed inverted matrix structure. A similar transformation from a colloidal crystal to an ordered macroporous matrix has been observed in copolymer sphere systems.[16] Accordingly, large spheres with diameters of ca. 140 nm generated from the O_h centers reside in these holes after 100 °C thermal treatment, as seen from SEM images (part D of Figure 7), whereas small spheres are engulfed inside the PMMA-rich matrix. Thermal treatment in nitrogen at

400 °C removes PMMA and F127 to yield the two sets of spherical particles.

Conclusion

This study has shown that syntheses based on combining triconstituent self-assembly with colloidal crystal templating provide good control over the morphology of porous products. While the systems studied here are compositionally complex, the parameters that yield a certain *external* morphology can be deciphered. Carbon, silica, or composite structures with hierarchical porosity (uniformly mesoporous walls surrounding periodic macropores) are reproducibly prepared as monolithic 3DOM/m pieces within certain precursor concentration ranges. For carbon, the monolith synthesis is significantly less laborious than a synthesis based on nanocasting, where a hierarchically structured silica preform has to be prepared first. Furthermore, the mesopore diameters and volumes in these carbon monoliths are considerably larger than those in nanocast carbon monoliths. Whereas previous triconstituent self-assembly reactions involved EISA of a dilute precursor mixture, here, a more concentrated triconstituent precursor solution was confined in the polymeric colloidal crystal, with no involvement of the EISA mechanism.

The continuous skeleton can be disconnected to produce shaped mesoporous nanoparticles, either by using a high triblock copolymer concentration or by employing an organic additive that acts both as a swelling agent for the surfactant template and as a plasticizer for the polymer colloidal crystal template. The mechanisms of disconnection are quite different for these two cases, and product shapes also differ. With a high surfactant concentration, the mesostructured walls become sufficiently weakened that the solid framework disassembles during calcination, forming cubic replicas of octahedral holes and smaller spheroidal particles originating from tetrahedral holes in the fcc colloidal crystal template (MSP-1). With an organic additive that can plasticize polymer spheres in the template, disconnection of the inorganic precursor seems to occur even before a solid skeleton is formed via fluid phase separation processes. As a result, both the large and the small mesoporous nanoparticles have spherical shapes. Even in this case, narrow product-size dispersions are achieved and internal mesopores are enlarged by the swelling agent. On the basis of SEM observations at each heat treatment stage, the unusual phase-separation mechanism that leads to the formation of MSP-2 particles involves liberation of TMB from surfactant micelles between 50–100 °C, causing the reconstruction of PMMA from a colloidal crystal to a macroporous network and isolating precursor regions within the PMMA/TMB phases. During this process, a number of interesting ordered patterns were observed for the mid-stage nanocomposites (parts A and D of Figure 7 and Figure S3 in the Supporting Information), which suggest that this self-assembly/

(54) Davis, M. E. *Nature* **2002**, *417*, 813–821.
(55) Henzie, J.; Barton, J. E.; Stender, C. L.; Odom, T. W. *Acc. Chem. Res.* **2006**, *39*, 249–257.

templating approach could be adapted in new low-cost nanofabrication methods.

For all of these nanocomposites, pure carbon or silica products were obtained after HF etching or combustion in air, respectively. We anticipate that these templating approaches can be generalized further to produce uniform, shaped nanoparticles of other compositions at nanometer and submicrometer length scales. In the case of nanocasting approaches, this has already been demonstrated,[14] but compositional modification may also be possible in direct syntheses. Future work will also be targeted at elucidating the role of composition and interfacial interactions on the *internal* pore architecture of the products. These uniform mesostructured particles may be used to assemble more complex nanostructures in multiple dimensions via bottom-up strategies for potential applications such as photonic devices[54] and nanoscale patterning.[55]

Supporting Information Available: SEM images of the original PMMA colloidal crystal template, MSP-1-C-SiO$_2$ particles carbonized at 1000 °C, MSP-2 after thermal treatment at 100 °C, and PMMA colloidal crystals treated with TMB. This material is available free of charge via the Internet at http://pubs.acs.org.

CM0717864